

# Geophysical Research Letters

## RESEARCH LETTER

10.1029/2019GL084246

### Key Points:

- We explore high-frequency spatiotemporal temperature variability in the Brazil-Malvinas Confluence using satellite and in situ data
- The shortest scales are associated with fronts and high mesoscale activity areas, while the largest ones occur along the Malvinas Current
- Subsurface variability is enhanced at the confluence, due to relatively small mesoscale features and numerous two-way thermohaline intrusions

### Supporting Information:

- Supporting Information S1

### Correspondence to:

D. Orúe-Echevarría and J. L. Pelegrí,  
dorleta.orue@gmail.com;  
pelegrí@icm.csic.es

### Citation:

Orúe-Echevarría, D., Castellanos, P., Sans, J., Emelianov, M., Vallès-Casanova, I., & Pelegrí, J. L. (2019). Temperature spatiotemporal correlation scales in the Brazil-Malvinas Confluence from high-resolution in situ and remote sensing data. *Geophysical Research Letters*, 46, 13,234–13,243. <https://doi.org/10.1029/2019GL084246>

Received 1 JUL 2019

Accepted 2 OCT 2019

Accepted article online 16 OCT 2019

Published online 26 NOV 2019

## Temperature Spatiotemporal Correlation Scales in the Brazil-Malvinas Confluence from High-Resolution In Situ and Remote Sensing Data

Dorleta Orúe-Echevarría<sup>1</sup> , Paola Castellanos<sup>2</sup> , Joel Sans<sup>3</sup>, Mikhail Emelianov<sup>1</sup> , Ignasi Vallès-Casanova<sup>1</sup> , and Josep L. Pelegrí<sup>1</sup> 

<sup>1</sup>Department d'Oceanografia Física i Tecnològica, Institut de Ciències del Mar, Consejo Superior de Investigaciones Científicas, Unidad Asociada ULPGC-CSIC, Barcelona, Spain, <sup>2</sup>Marine and Environmental Sciences Centre, Faculdade de Ciencias da Universidade de Lisboa, Lisbon, Portugal, <sup>3</sup>Unidad de Tecnología Marina, UTM-CSIC, Barcelona, Spain

**Abstract** Ocean frontal systems may act both as barriers and mixers between different water masses, the latter thanks to very energetic structures with relatively short temporal and spatial scales. Here, we explore the high-frequency temperature variability in the Brazil-Malvinas Confluence through the joint analysis of novel high-resolution SeaSoar measurements and sea surface temperature imagery. Surface spatiotemporal correlation scales range between 1.5 and 6 days and between 20 and 50 km, with the shortest scales along the shelf-break path of the Brazil Current and over the confluence and the longest ones along the Malvinas Current. The spatial scales display minima along the front, at the surface because of the presence of brackish shelf waters and at the subsurface due to both mesoscale and submesoscale thermohaline intrusions. The smallest cross-frontal vertical correlations, in the 5- to 10-m range, are associated with submesoscale processes. Overall, temperature variability is enhanced at depth in the frontal system.

**Plain Language Summary** The analysis of correlation scales may be used to recognize the spatial and temporal coherence of ocean properties, which allows identifying the main forcing mechanisms and dynamic processes in a certain oceanic region. This is of special relevance in frontal systems, which may possibly appear as barriers between different water masses but, because of enhanced activity with relatively short temporal and spatial scales, may also behave as water mixers. Here, we use high-resolution satellite imagery and in situ novel measurements to examine the temporal and spatial temperature correlation scales in the Southwest Atlantic Ocean; our focus is on the Brazil-Malvinas Confluence, a very intense open-ocean frontal system that has extraordinary importance in the global overturning circulation. Our results show that indeed the frontal system is the locus of high-frequency small-scale processes, which likely act as an efficient mechanism for the down-gradient transfer of properties. Further, these processes are smaller and faster at the subsurface (down to at least 200 m) than at the sea surface. Our results emphasize the necessity of understanding and monitoring these subsurface processes if we are to properly represent those regional processes that bear global implications.

## 1. Introduction

Frontal regions are characterized by multiple-scale turbulence (Fu, 2007; Lumpkin & Johnson, 2013). In the Southwest Atlantic Ocean, the dominant frontal system is the Brazil-Malvinas Confluence (BMC), generated at the encounter of the Brazil Current (BC) and Malvinas Current (MC; Figure 1). The meandering and retroflection of these currents leads to an intricate multiscale and highly energetic region, filled with mesoscale and submesoscale structures such as eddies, rings, filaments, and intrusions (Bianchi et al., 1993; Legeckis & Gordon, 1982; Lentini et al., 2002, 2006; Provost et al., 1999). Therefore, this region is thought to be characterized by short temporal and spatial scales of variability (Barré et al., 2006).

The MC (subantarctic) and BC (subtropical) waters present intense contrasts in sea surface height (SSH), primary production, and sea surface temperature (SST). These sharp gradients have allowed assessing the spatial and temporal variability of the surface BMC using satellite imagery (Garcia et al., 2004; Goni & Wainer, 2001; Gonzalez-Silveira et al., 2006; Goni et al., 2011; Machado et al., 2013; Saraceno et al., 2004, 2005). In particular, high SST horizontal gradients, of the order of 0.1°C/km, are found in the main frontal systems: the shelf-break Brazil region, the BMC front, the Subantarctic Front (SAF) and the Brazil Current Front

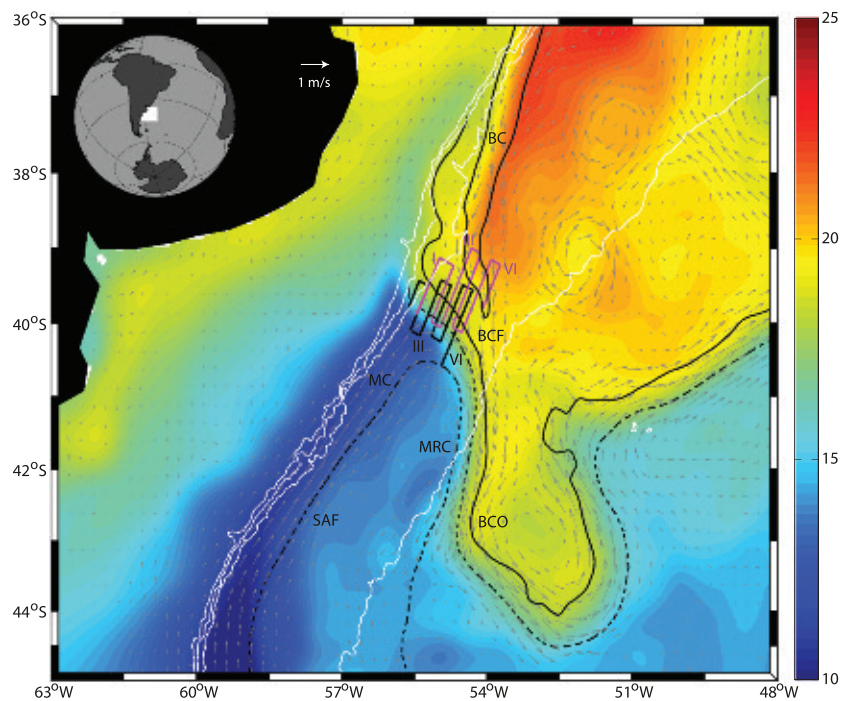


**Figure 1.** Mean sea surface temperature ( $^{\circ}\text{C}$ ) in the southwest Atlantic Ocean for 17–21 April 2017 as deduced from the Operational Sea Surface Temperature and Sea Ice Analysis data. The location of the SeaSoar1/SeaSoar2 survey tracks is shown by black/magenta lines, with Roman numbers indicating the cross-frontal transects for each survey. Grey vectors correspond to mean surface velocities from gridded altimetry for these days. Dashed black lines indicate the mean position of the Subantarctic Front (SAF, ADT =  $-0.05\text{ m}$ ) and Brazil Current Front (BCF, ADT =  $0.3\text{ m}$ ) as defined by Ferrari et al. (2017). Solid black lines indicate the position of the BCF based on sea surface temperature gradients following the methodology in Saraceno et al. (2004). White lines correspond to the 200-, 500-, 1,000-, and 5,000-m isobaths (GEBCO, 2008). The main streams are labeled: Brazil Current (BC), Malvinas Current (MC), Malvinas Return Current (MRC), and Brazil Current Overshoot (BCO).

(BCF; Saraceno et al., 2004). Less pronounced SST gradients also show up at the mesoscale and submesoscale structures formed downstream of the BMC (Barré et al., 2006).

Regarding surface temporal variability, most studies have focused on the semiannual and interannual scales, characterized by the migration of the latitude where the BC diverts from the shelf (Goni et al., 2011; Goni & Wainer, 2001; Olson et al., 1988). Synoptic variability has been associated with the regional and mesoscale structures, particularly with the position of the MC, the BC, and the BC overshoot (BCO; Goni & Wainer, 2001; Legeckis & Gordon, 1982). Garzoli and Garraffo (1989) and Ferrari et al. (2017) found that the BCO moves zonally with time scales of 90–150 days, and Provost and LeTraon (1993) have observed that the dominant mesoscale features have temporal and spatial scales of 75–150 days and 100–500 km. Higher frequency surface variations are also expected in the BMC, as for example, SST consecutive images show changes up to  $\pm 4^{\circ}\text{C}/\text{d}$  (Barré et al., 2006). One potential source is the changing winds that can flush shelf water over much of the frontal area, bringing potential temperature and salinity ( $\theta, S$ ) changes in only a few days (Combes & Matano, 2018; Guerrero et al., 2014). Other studies on thermohaline changes in the Patagonian shelf-break front have found 1- to 5-day correlation times for temperature in the upper 100 m, which have been associated with synoptic atmospheric storms (Carranza et al., 2017; Garzoli & Simionato, 1990; Valla & Piola, 2015).

Contrary to sea surface studies, the subsurface variability of  $\theta$  and  $S$  in the BMC remains barely explored. Paniagua et al. (2018) have reported  $\theta/S$  changes of  $0.3^{\circ}\text{C}/0.18$  in 3 days at a slope mooring in the path of the MC (near  $41^{\circ}\text{S}$  and 1000 m depth). This high-frequency variability has been ascribed to either the intense mesoscale activity of the region, with eddies translating at velocities between 1 and 10 km/d (Mason et al., 2017; Pilo et al., 2015) or to the east-west and north-south BMC migrations at speeds up to 10 km/d (Garzoli & Bianchi, 1987; Legeckis & Gordon, 1982). Subsurface rapid changes may also be caused by

thermohaline intrusions with lifetimes of 5–13 days (Bianchi et al., 1993, 2002) or baroclinic frontal instabilities oscillating with periods of 3–5 days (Garzoli & Simionato, 1990).

Subsurface structures may be largely decoupled from the surface fields due to the development of the seasonal thermocline (Provost et al., 1996; Saraceno et al., 2004) and the presence of localized thermohaline frontal intrusions (Orúe-Echevarría et al., 2019). However, their existence does influence the conditions at the sea surface, especially affecting the water elevation and velocity (Maamaatuaiahutapu et al., 1999). Hence, a proper knowledge of these subsurface scales is necessary not only to quantify the water transfer cross the frontal system, of major relevance in the large-scale redistribution of properties, but also to improve the design of operational models.

## 2. Data and Methods

The RETRO-BMC cruise was conducted onboard R/V Hespérides between 8 and 28 April 2017 in the BMC frontal region (Pelegrí et al., 2019). Here, we analyze data from 12 cross-frontal high-resolution transects aimed at finding the short temporal and spatial scales in the frontal region. These transects were done within 5 days, between 40.6°S–56.7°W and 39°S–53.6°W, as part of two surveys carried out with a winged and towed undulating platform (SeaSoar), which included temperature, salinity, and pressure sensors (Annex I, Supporting Information).

Each of the two SeaSoar surveys consisted of six near-parallel transects, ranging from 55 to 90 km long, with all tracks separated by 18 km (except tracks I and II of SeaSoar1, which were 27 km apart) and covering an area of approximately 135 km zonally and 100 km meridionally (Figure 1). The individual transects were oriented cross the frontal region, following tracks either 25° or 205° from the true north. The first survey (SeaSoar1, 17–18 April) covered 620 km and was completed within 46 hr; the second survey (SeaSoar2, 19–21 April) started 40 hr after completion of SeaSoar1 and extended over 751 km in 52 hr.

The temperature and salinity data were gathered as a function of pressure for all cross-frontal tracks as well as in the five short transects between them. These raw data were linearly binned to 1-dbar vertical intervals, every 5 km along the SeaSoar tracks following the methodology in Sans (2018). Finally, the potential temperature ( $\Theta$ ) field was calculated and interpolated horizontally onto a regular  $0.05^\circ \times 0.05^\circ$  grid; hereafter, whenever mentioning temperature, we will always implicitly refer to the potential values.

Both surveys were carried out from west to east, in the same direction of the mean flow over the frontal region, as an attempt to minimize aliasing effects. Considering the distance between the first and last cross-frontal transect (90–100 km) and the time of the survey (40–50 hr), it turns out that the vessel moved along the front with a mean speed of 0.5–0.7 m/s, similar to the characteristic along-front sea surface velocities (Figures 1 and S3, Supporting Information; Orúe-Echevarría et al., 2019). Further confidence on the results comes from the fact that during each survey, the frontal displacements were relatively small as compared with the extension of the cross-frontal tracks; the only large displacement occurred between 20 and 21 April 2017, in the western portion of the survey area, when the ship had already reached the eastern part of the domain (Figure S4).

In addition to hydrographic data, we also use two satellite datasets for April 2017: Operational Sea Surface Temperature and Sea Ice Analysis (OSTIA) SST and absolute dynamic topography (ADT, the difference of SSH and the geoid). The OSTIA SST combines in situ data with infrared and microwave satellite data. Both data sets are provided by the Copernicus Marine and Environment Monitoring Service (<http://marine.copernicus.eu>). The multiscale optimal interpolation scheme in the OSTIA SST product allows studying the frontal variability at temporal/horizontal scales larger than about 1 day/10 km (Donlon et al., 2012; Reynolds et al., 2013), while the ADT can only resolve temporal/horizontal scales longer than 20 days/40 km (Pujol et al., 2016).

The autocorrelation decreases with time and distance, over scales that depend both on external forcing and local dynamics (Sumata et al., 2018). A correlation scale can be defined as to characterize the prevailing temporal and spatial scales, with short scales identifying areas of high-frequency changes. Throughout this study, we fit the autocorrelation to a Gaussian function and define the correlations in terms of *e*-folding scales (Molinari & Festa, 2000; Annex II, Supporting Information). Using SST satellite data, we can determine the sea surface temporal and horizontal correlation scales. Similarly, the SeaSoar data allow

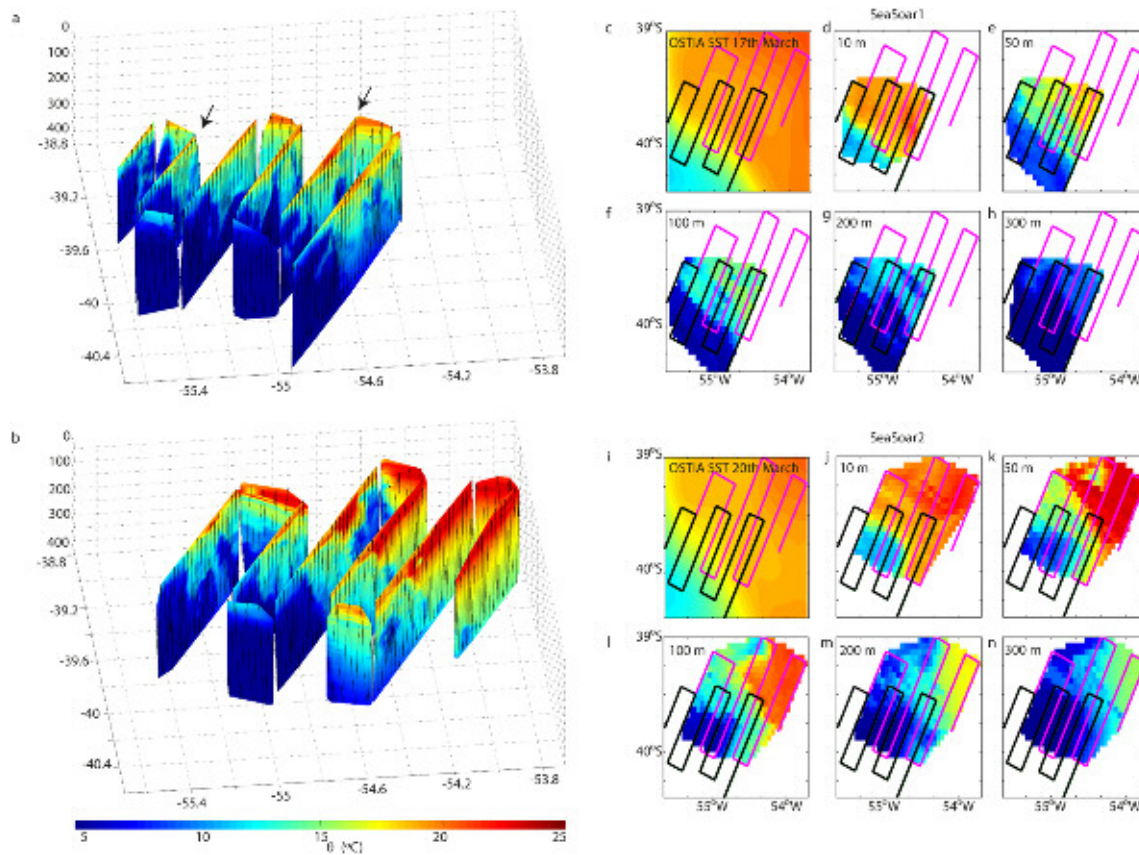


**Figure 2.** Three-dimensional temperature view during (a) SeaSoar1 and (b) SeaSoar2. The black vertical lines indicate the central point of the SeaSoar diving cycle. The black arrows show vertical sections II and V of SeaSoar1, used to illustrate the vertical correlation scales in Figure 4. OSTIA SST for the (c) 17 and (i) 20 April 2017. Horizontal temperature fields at 10, 50, 100, 200, and 300 m for (d–h) SeaSoar1 and (j–n) SeaSoar2. The location of the SeaSoar1/SeaSoar2 tracks is shown by black/magenta lines. (Additional horizontal temperature and salinity fields are shown in Figures S7 and S8). OSTIA = Operational Sea Surface Temperature and Sea Ice Analysis; SST = sea surface temperature.

estimating the horizontal correlation scales in the survey area and the vertical correlation scales along the cross-frontal sections. In contrast, the two SeaSoar provide temperature differences in about 3 days but do not allow calculating the temporal subsurface time correlation. The signal-to-noise ratio (SNR) in the autocorrelation functions is inferred from the fraction of explained variability (Sprintall & Meyers, 1991; Hosoda & Kawamura, 2004; Annex II, Supporting Information).

### 3. Results

#### 3.1. High-resolution Three-dimensional View of the Frontal System

The SST and surface geostrophic velocity fields show the MC flowing northward along the 500–1,000 isobaths and reaching 40°S with  $\theta < 10^\circ\text{C}$  and  $S < 34.5$ , where it encounters warmer and saltier subtropical waters (Figure 1). These velocity fields, together with the salinity and temperature sections (Figures 2, S5, and S6), also reveal the BC crossing the northeastern end of the study area and show relatively colder shelf waters covering most of the northern and western sections. Surface salinity values confirm the presence of widespread low-salinity shelf waters over the study area (Figures S5 and S7). East of 55°W, the BC follows south as a well-developed elongated BCO that reaches as far as 44°S and 51°W.

Figure 1 also shows the intricate confluence of the SAF and BCF in the BMC region, that is, the collision of the two boundary currents that leads to a single yet complex BMC frontal system. The three-dimensional  $\theta$  and  $S$  fields (Figures 2 and S5–S8) illustrate this complexity, with one main transition from subantarctic to subtropical waters at the isotherm/isohaline of  $12^\circ\text{C}/34.7$  and a second transition at the isotherm/isohaline of  $17^\circ\text{C}/35.3$ . Interestingly, the classical definition of the BCF (set to  $\text{ADT} = 0.3 \text{ m}$ ) coincides with the first

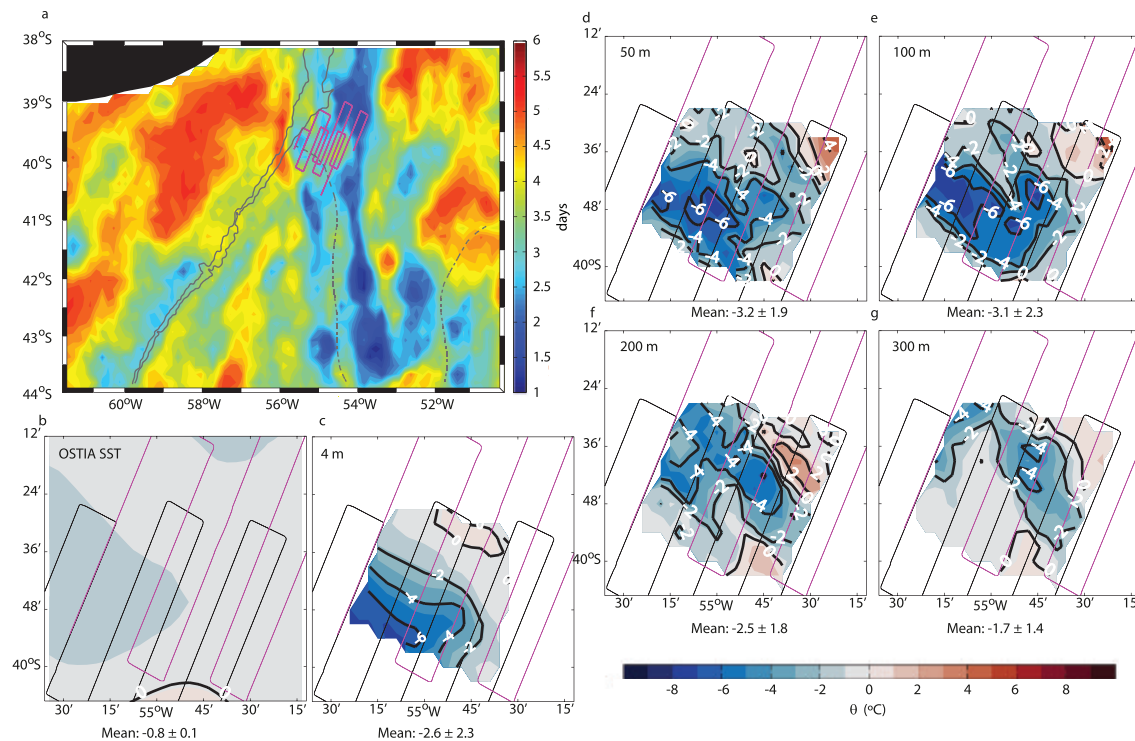


**Figure 3.** (a) OSTIA SST temperature temporal correlation scale (days); the black solid lines correspond to the 500 and 1,000 m isobaths, while the black dashed line indicates the mean position of the BCF for April 2017. (b) OSTIA SST difference between the 20 and 17 April 2017. Temperature differences between SeaSoar2 and SeaSoar1 at (c) 10, (d) 50, (e) 100, (f) 200, and (g) 300 m. Negative values denote cooling; in each panel, the mean  $\pm$  standard deviation temperature differences are indicated. The black/magenta lines show the SeaSoar1/SeaSoar2 tracks.

transition and the entire region between the first and second transition is the one that displays most of the interleaving. North of the second transition, which is observed on the northeastern end of the survey region (crossed by tracks III–VI of SeaSoar2), the subtropical waters remain fairly unperturbed.

The frontal system is characterized by substantial thermohaline intrusions. In the western stations (I–III in SeaSoar1 and I–II in SeaSoar2), the subantarctic side remains fairly immaculate, but the subtropical side displays mesoscale features. There are at least two tongues or wedges of subantarctic waters intruding into the subtropical region—a central one during SeaSoar1 and a western one during SeaSoar2—some 10–30 km wide and stretching by as much as 100 km (Figures 2d–2h, 2j–2n, S7, and S8). These subsurface tongues are smaller than the surface ones and have no surface expression in the SST and ADT images (Figures 1 and S3). In contrast, the eastern sections (IV–VI in SeaSoar1 and III–VI in SeaSoar2) reveal opposite sign submesoscale intrusions, that is, warm/cold in the subantarctic/subtropical sides of the front. All mesoscale and submesoscale intrusions are found between the 26.5 and 27.0 isopycnals, displaying temperature gradients sharper than at the sea surface (0.3–0.8°C/km; Figures S6 and S8).

### 3.2. Temporal Correlation Scales

For the entire Southwest Atlantic Ocean, the OSTIA SST temporal correlation scales range between 1.5 and 6 days (Figure 3a). The shortest scales (1.5–3.5 days) are associated with the shelf-break in subtropical waters, the BMC front and the BCO, that is, to frontal regions with intense currents and high mesoscale activity, characterized by elevated eddy kinetic energy and rapid migrations of the frontal structures (Figure S4; Legeckis & Gordon, 1982; Garzoli & Simionato, 1990; Saraceno & Provost, 2012). In other areas, including the MC and MRC, fewer mesoscale structures develop (Artana et al., 2016), leading to less variability, longer temporal correlation scales (5–6 days), and higher SNR (Figure S9a).

During April 2017 and in the limited region enclosing the SeaSoar survey area, the OSTIA SST temporal correlation scales range between 2 and 4.5 days, with a mean monthly value of  $3.0 \pm 0.2$  days (see the sampling window in Figure 3b). Over the SeaSoar survey tracks, the OSTIA SST differences between 17 and 20 April

(precisely 3 days) range between  $-1.9^{\circ}\text{C}$  and  $2.1^{\circ}\text{C}$ , with the greatest cooling over the western sections and slight warming south of the SeaSoar tracks. We may also use the entire April data to generate, at each grid point, time series of SST differences for 3-day intervals (not shown), when averaged over the SeaSoar survey area the mean standard deviation is  $1.1^{\circ}\text{C}$  and the mean maximum absolute difference is  $2.6^{\circ}\text{C}$ .

Both the OSTIA SST and 4-m SeaSoar temperature differences indicate cooling over the frontal region, though the SeaSoar data show greater values (Figures 3b and 3c); these discrepancies possibly reflect some level of near-surface homogenization due to a shallow summer mixed layer (Provost et al., 1996) and the spreading of brackish shelf waters over the frontal region but may also respond to an increased uncertainty caused by high cloud coverage in April 2017 (around 65%). The subsurface temperatures also display a generalized cooling between 17 and 20 April, with peak absolute values between 50 and 150 m (Figures 3d–3f). At 300 m, the peak absolute differences are smaller (yet reaching values similar to 10 m) and remain restricted to the central region, associated with the intrusion of subantarctic waters (Figure 3g).

The different character of the surface and subsurface fields in the frontal SeaSoar survey area is remarkable. The characteristic 3-day SST variability (mean  $1.1^{\circ}\text{C}$  and maximum  $2.6^{\circ}\text{C}$  from OSTIA for April and mean  $2.2^{\circ}\text{C}$  and maximum about  $5^{\circ}\text{C}$  from the 10-m SeaSoar data between 17 and 20 April) is substantially less than the mean values in the 50- to 150-m depth interval (mean  $2.8^{\circ}\text{C}$  and maximum about  $7^{\circ}\text{C}$  from the SeaSoar data between 17 and 20 April).

### 3.3. Vertical Correlation Scales

We examine the vertical correlation scales through both individual and ensemble SeaSoar cross-frontal sections. In every individual section, the distribution of the vertical correlation scales is patchy, with values ranging between 10 and 25 m (Figure S10). Low values are related to large vertical changes in temperature, either associated with the seasonal thermocline, with the edge of frontal structures or with intrusions of distinct water masses.

An inspection of all sections suggests that some differences are associated with the distance (and hence time) from the initial encounter of the MC and BC. In Figures 4a and 4b, we illustrate the results for two sections: one in the western boundary of the survey area, close to the encounter point of the BC and MC (section II of SeaSoar1), and the other in the eastern margin (section V of SeaSoar1). The small correlation lengths (8–12 m) correspond roughly to those bands of high background vertical stratification; the SNR is large over the entire domain, generally above 3 and reaching 7 in the unperturbed well-stratified subtropical waters (see Figure S9b, for section II of SeaSoar1). In the western section, the subantarctic side of the frontal system displays relatively high correlation values, indicative of the absence of intrusions, while the subtropical side shows some large features, about 50–80 m thick and 60 km long (Figure 4a). In the eastern section, we still find some large features in the subtropical side, but there are also small intrusions on both sides of the frontal system, some 10–50 m thick and 10–20 km long (Figure 4b).

In order to best identify the longitudinal differences, we divide the sections into western (sections I–III in SeaSoar1 and I and II in SeaSoar2), close to the shelf-break confluence point, and eastern (all other seven sections), where the two colliding currents have been in close contact for a longer time. The division is set about 55 km offshore from the 500-m isobath, which we consider as the shelf-break emergence of the confluence (see the bathymetry and location of the BCF in Figure 1); considering along-front mean velocities of 0.5–1 m/s (Orúe-Echevarría et al., 2019), this represents that the water masses reaching the eastern sections have been in contact for at least an additional 15–30 hr. Following this separation, we produce ensemble sections with the origin referenced to the location of the BCF, defined as the point where the  $10^{\circ}\text{C}$  isotherm crosses 200 m (Garzoli & Bianchi, 1987). In this way, there are five western and seven eastern realizations (one of the eastern sections did not cross the BCF) that can be combined to compute the mean and standard deviation of the vertical correlation at each cross-frontal coordinate and depth.

In Figures 4c and 4d, we show the mean (obtained using a 10-m low-pass vertical filter) and standard deviation of the vertical correlation scales; only the portion of the vertical section with three or more realizations is shown. The two ensemble sections have fairly similar mean values (14–18 m). The main difference appears in the standard deviations: the western section shows a clear contrast across the front, between small values in the subantarctic side versus high values in the subtropical side; contrarily, the eastern section shows little difference between both sides of the front, with substantially greater intermittency. These results are consistent

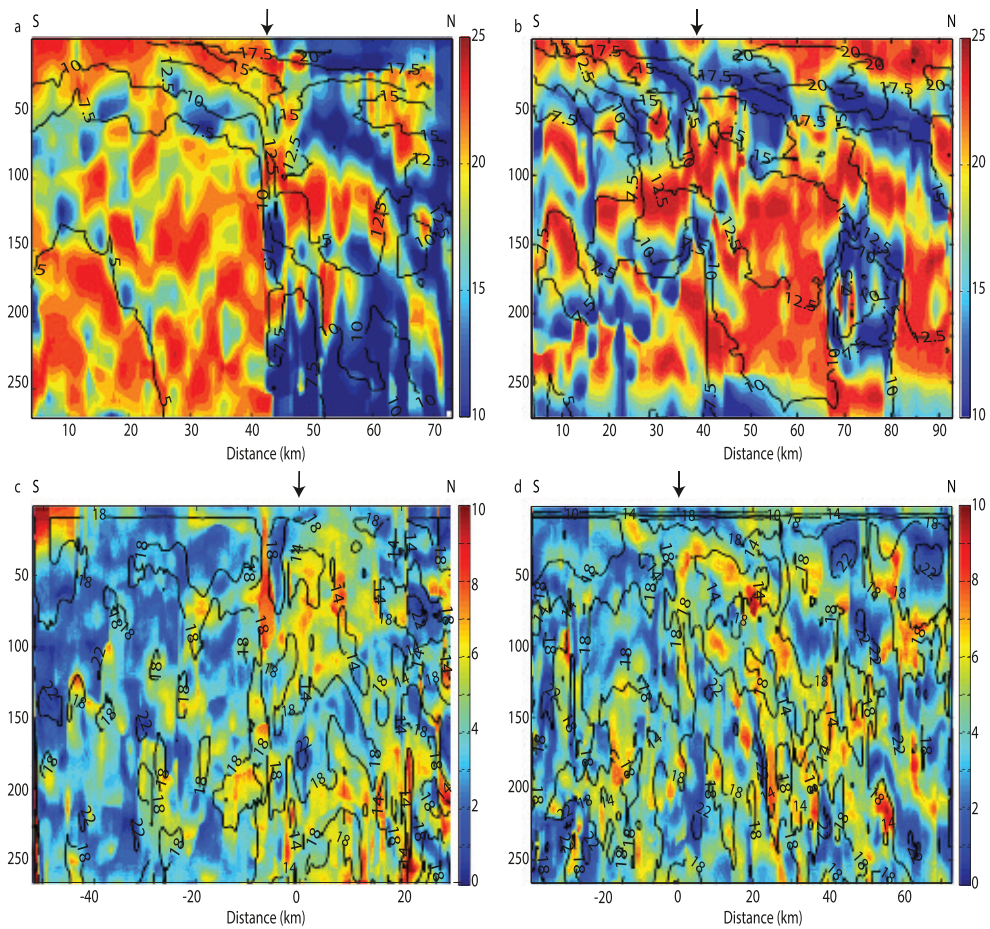


**Figure 4.** Vertical correlation scales (m) for (a) section II and (b) section V of SeaSoar1; black contours represent isotherms ( $^{\circ}$ C). Mean (black contours) and standard deviation (colored) of the vertical correlation scales (m) for the (c) western and (d) eastern stations. The black arrows show the position of the front.

with the view of the frontal system as the locus of subsurface mesoscale incursions at any position (in section 3.1, we pointed at the existence of cold-fresh subsurface tongues of subantarctic waters penetrating northwards in the western and central tracks) and submesoscale thermohaline intrusions developing in the central and eastern sections. These submesoscale intrusions appear to be enhanced after the two water masses have been in contact for a sufficiently long time, of the order of one inertial period or 19 hr in our survey area (Shcherbina et al., 2010), either because of the inherent instability of the frontal region or as a result of the high salt-fingering activity in the BMC (Bianchi et al., 2002).

### 3.4. Horizontal Correlation Scales

We first examine the sea surface horizontal correlation lengths for the extended BMC region during April 2017, as deduced using the OSTIA SST fields (Figures 5a and 5b). The maximum correlations (major axes of the correlation ellipses) follow the pathway of the western boundary currents and its interior retroflections, ranging between about 35 and 55 km. Over the shelf and in the eastern portion of the domain, these values decrease, ranging between 20 and 30 km. The situation reverses for the minimum correlation lengths (minor axes), with the largest values occurring over the platform and the smallest ones taking place along the path of the major currents. Both results indicate that the boundary currents are largely asymmetric, with the longest correlation lengths well aligned with the current, while the shelf and other interior regions of high kinetic energy are dominated by shorter scales and more symmetric features (Figure S11). The SNR is fairly low, always less than 1.5, slightly less than the mean values found by Hosoda and Kawamura (2004) using microwave SST images (Figure S9); the largest SNR values occur over the platform and along the pathway of the MC.

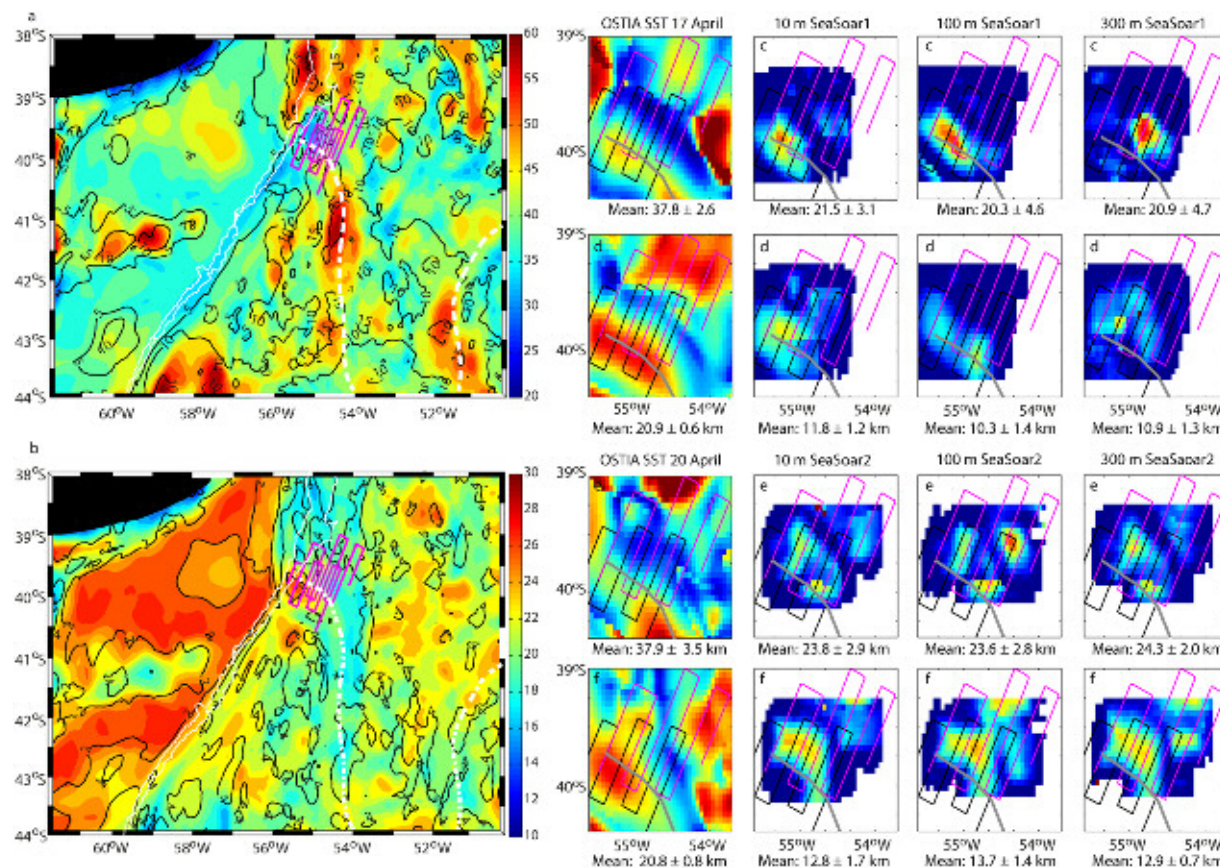


**Figure 5.** (a) Major and (b) minor axis lengths of the correlation ellipses, calculated using the April 2017 OSTIA SST data (the colors indicate the mean values and the black contours the standard deviation); the white thick-dashed line indicates the mean position of the Brazil Current Front for April 2017. Correlation-ellipse values: major axis lengths for (c) the OSTIA SST on 17 April and SeaSoar1 and (e) the OSTIA SST on 20 April and SeaSoar2, color coded as in (a); minor axis lengths for (d) the OSTIA SST on 17 April and SeaSoar1 and (f) the OSTIA SST on 20 April and SeaSoar2, color coded as in (b); the SeaSoar data is at 10, 100, and 300 m, as indicated, and the grey line shows the position of the BCF on 17 April (c, d) and 21 April (e, f). The black/magenta lines show the SeaSoar1/SeaSoar2 tracks, the white solid lines correspond to the 500- and 1,000-m isobaths. OSTIA = Operational Sea Surface Temperature and Sea Ice Analysis; SST = sea surface temperature.

Over the SeaSoar survey area, the situation differs substantially at the surface and subsurface (Figures 5c–5f, S11c, S12, and S13). The OSTIA SST field displays a band of minimum major and minor axis correlation lengths along the frontal system (less than 25/15 km for the major/minor axes), surrounded by values that are at least twice as large. In contrast, the subsurface SeaSoar data is noisy but shows fairly large values south of the front (40–50 km for the major axis), in the subantarctic water domain, and much smaller values along and north of the front (20–30 km for the major axis); nevertheless, the correlations in the southern domain decrease as we move away from the slope, consistent with the idea of thermohaline intrusions developing when the two water masses remain in contact for long enough (section 3.3). Remarkably, the band of minimum surface values is included in the southern portion of subsurface maximum values, sustaining the idea that this narrow surface band responds to brackish and relatively cold platform waters stretching along the southern sector of the front (Orúe-Echevarría et al., 2019). This is confirmed by the surface salinity values (Figures S5 and S7).

#### 4. Conclusions

We have combined high-resolution remote-sensing surface and SeaSoar survey subsurface temperature data to explore the structure of the BMC, a very dynamic and intricate open-ocean frontal system. The spatial resolution of both data sets is about 5 km, although the spatial coverage of the subsurface data is much smaller. The temporal resolution of the surface remote-sensing data is 1 day, while for the subsurface data, we only have two (3 days apart) realizations.

At the sea surface, the large areal coverage of the SST data allows separating the shelf and deep-ocean regions. Over the shelf, the temporal correlations are relatively large (5 days), yet the spatial correlations are moderate (40 km) except in the northern shelf (50–55 km). These results reflect that, except for the northern margin off La Plata River, the entire shelf is characterized by weak currents. Off the shelf, the results display three major regions: (1) the MC and its retroflection, characterized by long temporal (4–5 days) and spatial (40–60 km) correlations, as expected for an intense and coherent current with relatively few mesoscale features; (2) the BC and its overshoot, represented by short temporal (1.5–3.5 days) but long spatial (40–60 km) correlations, as foreseen for an intense but more intermittent current, with substantial mesoscale variability; (3) the interior ocean away from the boundary currents, depicted by relatively long temporal (5–6 days) and short spatial (25–45 km) correlations, reflecting smaller and less energetic structures.

The SeaSoar data permits having a closer look at the frontal region. The surface waters display both low temporal (1.5–4 days) and spatial (20–30 km) correlations, with an outstanding narrow band of minimum spatial correlation values, which we ascribe to brackish filaments stretching from the shelf along the front. At the subsurface, the front is characterized by relatively long/short spatial correlations in its southern/northern sides (40–50 vs. 20–30 km), although the southern correlation distances decrease as we move away from the slope. These values are consistent with the idea of two colliding water masses, with small mesoscale intrusions of subantarctic water at the collision and the downstream development of both sign submesoscale thermohaline intrusions. Further comparison of the surface and subsurface patterns shows that subantarctic waters are located right below the brackish filament.

The vertical correlation scales reflect the seasonal thermocline, the frontal structure, and the presence of intrusions. The values range between 10 and 25 m, with the longest distances occurring in the subantarctic waters close to the shelf. The observed subsurface distributions are again consistent with the presence of mesoscale tongues of subantarctic waters close to the slope, penetrating north through the front, and submesoscale thermohaline intrusions further offshore.

Our results point at the frontal system as the locus of high-frequency small-scale processes, leading to the down-gradient transfer of properties. These subsurface processes, which are smaller and faster at the subsurface (down to at least about 200 m) than at the sea surface, are hardly represented in operational models. An improved representation of the intrusion dynamics in frontal systems is needed if we wish to properly typify those subsurface processes that bear global implications.

## Acknowledgments

We are very grateful to the crew of R/V Hespérides and the scientific and technical teams for their vital help during the RETRO-BMC cruise. We are also thankful to our two anonymous reviewers for their constructive and useful comments and suggestions. We acknowledge funding from the Spanish Government through projects VA-DE-RETRO (CTM2014-56987-P) and SAGA (RTI2018-100844-B-C33). D. O. E. was funded through an FPU contract and I. V. C. through and FPI contract. In situ SeaSoar data are available for download at Pelegrí et al. (2019; <https://digital.csic.es/handle/10261/188363>). Satellite SST and altimetry data are available at Copernicus Marine Environment monitoring service (CMEMS; <http://marine.copernicus.eu/>).

## References

- Artana, C., Ferrari, R., Koenig, Z., Saraceno, M., Piola, A. R., & Provost, C. (2016). Malvinas Current variability from Argo floats and satellite altimetry. *Journal of Geophysical Research: Oceans*, 121, 4854–4872. <https://doi.org/10.1002/2016JC011889>
- Barré, N., Provost, C., & Saraceno, M. (2006). Spatial and temporal scales of the Brazil–Malvinas Current confluence documented by simultaneous MODIS Aqua 1.1-km resolution SST and color images. *Advances in Space Research*, 37(4), 770–786. <https://doi.org/10.1016/j.asr.2005.09.026>
- Bianchi, A. A., Giulivi, C. F., & Piola, A. R. (1993). Mixing in the Brazil–Malvinas confluence. *Deep Sea Research Part I: Oceanographic Research Papers*, 40(7), 1345–1358. [https://doi.org/10.1016/0967-0637\(93\)90115-J](https://doi.org/10.1016/0967-0637(93)90115-J)
- Bianchi, A. A., Piola, A. R., & Collino, G. J. (2002). Evidence of double diffusion in the Brazil–Malvinas Confluence. *Deep Sea Research Part I: Oceanographic Research Papers*, 49(1), 41–52. [https://doi.org/10.1016/S0967-0637\(01\)00039-5](https://doi.org/10.1016/S0967-0637(01)00039-5)
- Carranza, M. M., Gille, S. T., Piola, A. R., Charo, M., & Romero, S. I. (2017). Wind modulation of upwelling at the shelf-break front off Patagonia: Observational evidence. *Journal of Geophysical Research: Oceans*, 122, 2401–2421. <https://doi.org/10.1002/2016JC012059>
- Combes, V., & Matano, R. P. (2018). The Patagonian shelf circulation: Drivers and variability. *Progress in Oceanography*, 167, 24–43. <https://doi.org/10.1016/j.pocean.2018.07.003>
- Donlon, C. J., Martin, M., Stark, J., Roberts-Jones, J., Fiedler, E., & Wimmer, W. (2012). The Operational Sea Surface Temperature and Sea Ice Analysis (OSTIA) system. *Remote Sensing of Environment*, 116, 140–158. <https://doi.org/10.1016/j.rse.2010.10.017>
- Ferrari, R., Artana, C., Saraceno, M., Piola, A. R., & Provost, C. (2017). Satellite Altimetry and Current-Meter Velocities in the Malvinas Current at 41°S: Comparisons and modes of variations. *Journal of Geophysical Research: Oceans*, 122, 9572–9590. <https://doi.org/10.1002/2017JC013340>
- Fu, L.-L. (2007). Interaction of mesoscale variability with large-scale waves in the Argentine Basin. *Journal of Physical Oceanography*, 37(3), 787–793. <https://doi.org/10.1175/JPO2991.1>
- García, C. A. E., Sarma, Y. V. B., Mata, M. M., & García, V. T. M. (2004). Chlorophyll variability and eddies in the Brazil–Malvinas Confluence region. *Deep Sea Research Part I: Oceanographic Research Papers*, 51, 159–172. <https://doi.org/10.1016/j.dsri.2003.07.016>
- Garzoli, S., & Simionato, C. (1990). Baroclinic instabilities and forced oscillations in the Brazil/Malvinas confluence front. *Deep Sea Research Part A: Oceanographic Research Papers*, 37(6), 1053–1074. [https://doi.org/10.1016/0198-0149\(90\)90110-H](https://doi.org/10.1016/0198-0149(90)90110-H)
- Garzoli, S. L., & Bianchi, A. (1987). Time-space variability of the local dynamics of the Malvinas–Brazil confluence as revealed by inverted echo sounders. *Journal of Geophysical Research*, 92(C2), 1914–1922. <https://doi.org/10.1029/JC092iC02p01914>
- Garzoli, S. L., & Garraffo, Z. (1989). Transports, frontal motions and eddies at the Brazil–Malvinas currents confluence. *Deep Sea Research Part A: Oceanographic Research Papers*, 36(5), 681–703. [https://doi.org/10.1016/0198-0149\(89\)90145-3](https://doi.org/10.1016/0198-0149(89)90145-3)

- Goni, G. J., Bringas, F., & DiNezio, P. N. (2011). Observed low frequency variability of the Brazil Current front. *Journal of Geophysical Research*, 116, C10037. <https://doi.org/10.1029/2011JC007198>
- Goni, G. J., & Wainer, I. (2001). Investigation of the Brazil Current front variability from altimeter data. *Journal of Geophysical Research*, 106(C12), 31,117–31,128. <https://doi.org/10.1029/2000JC000396>
- Gonzalez-Silveira, A., Santamaría-del-Angel, E., & Millán-Núñez, R. (2006). Spatial and temporal variability of the Brazil-Malvinas Confluence and the La Plata Plume as seen by SeaWiFS and AVHRR imagery. *Journal of Geophysical Research*, 111, C06010. <https://doi.org/10.1029/2004JC002745>
- Guerrero, R. A., Piola, A. R., Fenco, H., Matano, R. P., Combes, V., Chao, Y., et al. (2014). The salinity signature of the cross-shelf exchanges in the Southwestern Atlantic Ocean: Satellite observations. *Journal of Geophysical Research: Oceans*, 119, 7794–7810. <https://doi.org/10.1002/2014JC010113>
- Hosoda, K., & Kawamura, H. (2004). Global space-time statistics of sea surface temperature estimated from AMSR-E data. *Geophysical Research Letters*, 31, L72021. <https://doi.org/10.1029/2004GL020317>
- Legeckis, R., & Gordon, A. L. (1982). Satellite observations of the Brazil and Falkland currents—1975, 1976, and 1978. *Deep Sea Research Part A: Oceanographic Research Papers*, 29(3), 375–401. [https://doi.org/10.1016/0198-0149\(82\)90101-7](https://doi.org/10.1016/0198-0149(82)90101-7)
- Lentini, C. A. D., Goni, G. J., & Olson, D. B. (2006). Investigation of Brazil Current rings in the confluence region. *Journal of Geophysical Research*, 111, C06013. <https://doi.org/10.1029/2005JC002988>
- Lentini, C. A. D., Olson, D. B., & Podestá, G. P. (2002). Statistics of Brazil Current rings observed from AVHRR: 1993 to 1998. *Geophysical Research Letters*, 29(16), 1811. <https://doi.org/10.1029/2002GL015221>
- Lumpkin, R., & Johnson, G. C. (2013). Global ocean surface velocities from drifters: Mean, variance, El Niño–Southern Oscillation response, and seasonal cycle. *Journal of Geophysical Research: Oceans*, 118, 2992–3006. <https://doi.org/10.1002/jgrc.20210>
- Maamaatuaiahutapu, K., Provost, C., Andrié, C., & Vigan, X. (1999). Origin and ages of mode waters in the Brazil-Malvinas Confluence region during austral winter 1994. *Journal of Geophysical Research*, 104(C9), 21,051–21,061. <https://doi.org/10.1029/1999JC900177>
- Machado, I., Barreiro, M., & Calliari, D. (2013). Variability of chlorophyll-a in the Southwestern Atlantic from satellite images: Seasonal cycle and ENSO influences. *Continental Shelf Research*, 53, 102–109. <https://doi.org/10.1016/j.csr.2012.11.014>
- Mason, E., Pascual, A., Gaube, P., Ruiz, S., Pelegrí, J. L., & Delepouille, A. (2017). Subregional characterization of mesoscale eddies across the Brazil-Malvinas Confluence. *Journal of Geophysical Research: Oceans*, 122, 3329–3357. <https://doi.org/10.1002/2016JC012611>
- Molinari, R. L., & Festa, J. F. (2000). Effect of subjective choices on the objective analysis of sea surface temperature data in the tropical Atlantic and Pacific oceans. *Oceanologica Acta*, 23(1), 3–14. [https://doi.org/10.1016/S0399-1784\(00\)00108-0](https://doi.org/10.1016/S0399-1784(00)00108-0)
- Olson, D. B., Podestá, G. P., Evans, R. H., & Brown, O. B. (1988). Temporal variations in the separation of Brazil and Malvinas Currents. *Deep Sea Research Part A: Oceanographic Research Papers*, 35(12), 1971–1990. [https://doi.org/10.1016/0198-0149\(88\)90120-3](https://doi.org/10.1016/0198-0149(88)90120-3)
- Orué-Echevarría, D., Pelegrí, J. L., Machín, F., Hernández-Guerra, A., & Emelianov, M. (2019). Inverse Modeling the Brazil-Malvinas Confluence. *Journal of Geophysical Research: Oceans*, 124, 527–554. <https://doi.org/10.1029/2018JC014733>
- Paniagua, G. F., Saraceno, M., Piola, A. R., Guerrero, R., Provost, C., Ferrari, R., et al. (2018). Malvinas Current at 40°S–41°S: First assessment of temperature and salinity temporal variability. *Journal of Geophysical Research: Oceans*, 123, 5323–5340. <https://doi.org/10.1029/2017JC013666>
- Pelegrí, J. L., Orué-Echevarría, D., Castellanos, P., Guallar, C., Marotta, H., Marrasé, C., et al. (2019). The RETRO-BMC cruise onboard the R/V Hespérides, April 2017, Brazil-Malvinas Confluence: Hydrographic and drifters data. Digital CSIC. <https://doi.org/10.20350/digitalCSIC/8951>
- Pilo, G. S., Mata, M. M., & Azevedo, J. L. L. (2015). Eddy surface properties and propagation at Southern Hemisphere western boundary current systems. *Ocean Science*, 11(4), 629–641. <https://doi.org/10.5194/os-11-629-2015>
- Provost, C., Escoffier, C., Maamaatuaiahutapu, K., Kartavtseff, A., & Garçon, V. (1999). Subtropical mode waters in the South Atlantic Ocean. *Journal of Geophysical Research*, 104(C9), 21,033–21,049. <https://doi.org/10.1029/1999JC900049>
- Provost, C., Garçon, V., & Falcon, L. M. (1996). Hydrographic conditions in the surface layers over the slope-open ocean transition area near the Brazil-Malvinas confluence during austral summer 1990. *Continental Shelf Research*, 16(2), 215–235. [https://doi.org/10.1016/0278-4343\(95\)00006-M](https://doi.org/10.1016/0278-4343(95)00006-M)
- Provost, C., & LeTraon, P.-Y. (1993). Spatial and temporal scales in altimetric variability in the Brazil-Malvinas current confluence region: Dominance of the semiannual period and large spatial scales. *Journal of Geophysical Research*, 98(C10), 18,037–18,051. <https://doi.org/10.1029/93JC00693>
- Pujol, M.-I., Faugère, Y., Taburet, G., Dupuy, S., Pelloquin, C., Ablain, M., & Picot, N. (2016). DUACS DT2014: The new multi-mission altimeter data set reprocessed over 20 years. *Ocean Science*, 12, 1067–1090. <https://doi.org/10.5194/os-12-1067-2016>
- Reynolds, R. W., Chelton, D. B., Roberts-Jones, J., Martin, M. J., Menemenlis, D., & Merchant, C. J. (2013). Objective determination of feature resolution in two sea surface temperature analyses. *Journal of Climate*, 26(8), 2514–2533. <https://doi.org/10.1175/JCLI-D-12-00787.1>
- Sans, J. (2018). Metodología de reconstrucción de estructuras frontales. (Master's thesis, Universitat Oberta de Catalunya). Retrieved from <http://openaccess.uoc.edu/webapps/o2/handle/10609/83707?mode=full>
- Saraceno, M., & Provost, C. (2012). On eddy polarity distribution in the southwestern Atlantic. *Deep Sea Research Part I: Oceanographic Research Papers*, 69, 62–69. <https://doi.org/10.1016/j.dsr.2012.07.005>
- Saraceno, M., Provost, C., & Piola, A. R. (2005). On the relationship between satellite-retrieved surface temperature fronts and chlorophyll a in the western South Atlantic. *Journal of Geophysical Research*, 110, C11016. <https://doi.org/10.1029/2004JC002736>
- Saraceno, M., Provost, C., Piola, A. R., Bava, J., & Gagliardini, A. (2004). Brazil Malvinas Frontal System as seen from 9 years of advanced very high resolution radiometer data. *Journal of Geophysical Research*, 109, C05027. <https://doi.org/10.1029/2003JC002127>
- Shcherbina, A. Y., Gregg, M. C., Alford, M. H., & Harcourt, R. R. (2010). Three-Dimensional Structure and Temporal Evolution of Submesoscale Thermohaline Intrusions in the North Pacific Subtropical Frontal Zone. *Journal of Physical Oceanography*, 40, 1669–1689. <https://doi.org/10.1175/2010JPO4373.1>
- Sprintall, J., & Meyers, G. (1991). An optimal XBT sampling network for the eastern Pacific Ocean. *Journal of Geophysical Research*, 96(C6), 10,539–10,552. <https://doi.org/10.1029/91JC00274>
- Sumata, H., Kauker, F., Karcher, M., Rabe, B., Timmermans, M. L., Behrendt, A., et al. (2018). Decorrelation scales for Arctic Ocean hydrography – Part I: Amerasian Basin. *Ocean Science*, 14(1), 161–185. <https://doi.org/10.5194/os-14-161-2018>
- Valla, D., & Piola, A. R. (2015). Evidence of upwelling events at the northern Patagonian shelf break. *Journal of Geophysical Research: Oceans*, 120, 7635–7656. <https://doi.org/10.1002/2015JC011002>
- GEBCO (General Bathymetric Chart of the Oceans). (2008). GEBCO\_08 Grid, version 20100927. <http://www.gebco.net>